

Piecewise Planar Hulls for Semi-Supervised Learning of 3D Shape and Pose from 2D Images

Yigit Baran Can¹ Alexander Liniger¹ Danda Pani Paudel¹ Luc Van Gool^{1,2}

¹Computer Vision Lab, ETH Zurich ²VISICS, ESAT/PSI, KU Leuven

{yigit.can, alex.liniger, paudel, vangoool}@vision.ee.ethz.ch

Abstract

We study the problem of estimating 3D shape and pose of an object in terms of keypoints, from a single 2D image. The shape and pose are learned directly from images collected by categories and their partial 2D keypoint annotations. In this work, we first propose an end-to-end training framework for intermediate 2D keypoints extraction and final 3D shape and pose estimation. The proposed framework is then trained using only the weak supervision of the intermediate 2D keypoints. Additionally, we devise a semi-supervised training framework that benefits from both labeled and unlabeled data. To leverage the unlabeled data, we introduce and exploit the piece-wise planar hull prior of the canonical object shape. These planar hulls are defined manually once per object category, with the help of the keypoints. On the one hand, the proposed method learns to segment these planar hulls from the labeled data. On the other hand, it simultaneously enforces the consistency between predicted keypoints and the segmented hulls on the unlabeled data. The enforced consistency allows us to efficiently use the unlabeled data for the task at hand. The proposed method achieves comparable results with fully supervised state-of-the-art methods by using only half of the annotations. Our source code will be made publicly available.

1. Introduction

Estimating the shape and pose of an object in terms of pre-defined keypoints is a popular approach with wide range of applications such as registration [23, 29, 30, 58], recognition [17, 41] and generation [48, 59]. Apart from its use in human pose estimation and analysis [3, 4, 33, 43], keypoint-based shape representations are also useful in non-human object categories [10, 34, 44, 56], e.g., many applications including robotics and augmented reality require both 3D shape and pose [52].

Existing method for 3D shape and pose estimation [46, 47, 52, 61] use different forms of supervisions such as 3D

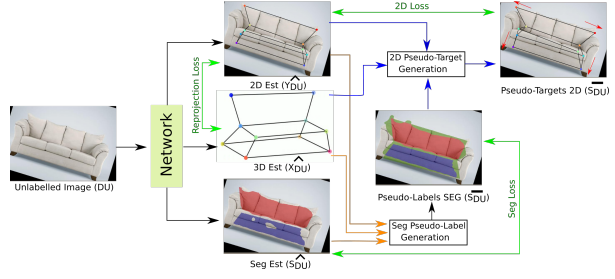


Figure 1. Our method outputs three predictions, $\hat{\mathbf{X}}$, $\hat{\mathbf{Y}}$ and $\hat{\mathbf{S}}$. The $\hat{\mathbf{X}}$ predication branch is self-supervised using the reprojection loss. Similarly, $\hat{\mathbf{Y}}$, and $\hat{\mathbf{S}}$ prediction branches are self-supervised using the pseudo-labels generated by the proposed 2D and semantic modules in the form of 2D and segmentation losses, respectively. Green pixels in the segmentation correspond to “uncertain” pixels.

keypoints, pose, or multiple views. Some methods [42, 57] also use 3D template-matching to match the 2D keypoints for the same object, however, they are known to be prone to occlusions [11]. Another set of methods directly estimates 3D locations of keypoints from a single image and therefore promises a much wider range of applications [14, 31]. One branch of these learning based methods uses a per-object-category image collection with 2D keypoint annotations to train a model which, during inference, can output 3D shape and pose from a single image. These methods are also called deep non-rigid structure-from-motion (NrSfM) due to their handling of image collections as images of an object under non-rigid transformation and different camera poses.

NrSfM methods can be divided into single category [26, 39, 60] and multiple category [34, 54] methods. Unlike single category methods which train a different model for each category, multi-category methods are computationally efficient in both training and testing. Therefore, we are interested to perform deep NrSfM in the multi-category setup directly from images, in an end-to-end manner. Note that most existing methods treat the 2D keypoints extraction and lifting them into 3D differently [7, 26, 34, 39, 54, 60], except [39], which only deals with human pose estimation.

The multi-category shape and pose estimation task re-

quires a large amount of 2D keypoint annotated images. This is one of the reasons that most existing methods use a pre-trained keypoint detector such as stacked-hourglass networks [51]. The need for large amounts of annotations for each additional object category significantly hinders the real world applicability of existing methods. Therefore, semi-supervised methods in this context are highly desirable. The few existing semi-supervised methods either require 3D annotations [53] or learn only the pose from pose annotations [19]. Up to our knowledge, there exists no semi-supervised method in the context of deep NrSfM. In this work, we propose the first semi-supervised method for deep NrSfM which exploits our piece-wise planar hulls prior of the object categories of interest. The proposed framework is illustrated in Figure 1.

We define the piece-wise planar hulls directly on the shape template, which is later on used to derive the semantic regions on the images. In simple terms, the planar hulls are lists that indicate which keypoints form a clique. We choose these cliques such that they represent some semantically meaningful surfaces in 3D. We perform the 2D segmentation of these semantic surfaces in an attempt to learn from contextual visual cues. The performed segmentation is ensured to be consistent to the predicted keypoints during the learning process. It is important to note that the planar hulls need to be defined only once per category, requiring an insignificant annotation effort.

Our weak and semi-supervised learning scheme exploits, (i) a partial labels of 2D keypoints for weak supervision using the labelled data, and (ii) cross-consistency between keypoints and planar hulls for self-supervision using the unlabelled data. For the latter purpose, we derive the pseudo-labels using the proposed 2D pseudo-target generation and segmentation pseudo-label generation modules, as shown in Figure 1. Such pseudo-labeling schema are widely used in the literature for various tasks [8, 13, 20, 32, 64, 65]. The pseudo-label generation process however requires careful design to be effective. Therefore, in this work, we develop several techniques to generate effective pseudo-levels, for the task at hand.

In summary, the major contributions of our work can be listed as follows:

- We introduce the concept of piece-wise planar hulls which can be defined using only the keypoints. The introduced planar hulls cover visually separable semantic regions.
- We propose the first semi-supervised method for deep NrSfM. In our approach, we exploit the cross consistency between the predicted semantic regions and the keypoints.
- Our semi-supervised method results a comparative performance compared to fully supervised state-of-the-art methods, using only 50% of labels on the PASCAL3D+

dataset.

2. Related Work

The field of NrSfM deals with estimating 3D locations of pre-determined keypoints as well as viewpoints for a set of observations of a particular object [1]. The problem has been studied extensively [2, 12, 25, 36, 62, 63]. By treating individual observations of different objects from the same category as different observations of a single object, deep NrSfM can be used to obtain 3D pose and shape from a single observation [6, 26, 27].

Some methods output the 3D structure of an object given only its image as meshes [22, 24]. While recent methods can estimate non-rigid meshes from multiple viewpoints, they work with objects of limited diversity, such as faces [21, 40, 55]. C3DPO [35] can output 3D shape and pose of a wide variety of classes by learning a decoupled canonical shape and viewpoint. Park et al. utilizes Procrustean regression [38] to determine unique motions and shapes [39]. While they also propose an end-to-end method that can output 3D keypoints from an image, their method only works with humans and cannot handle occlusions. Human pose estimation was also tackled in [7] by utilizing a cyclic-consistency loss. Recently, [54] extended Procrustean formulation with autoencoders and proposed a method that can infer 3D shapes without the need for sequence. However, their method accepts 2D keypoints as input rather than images and tackles the problem of obtaining 3D keypoint locations from a single image using a separate keypoint detector, such as a stacked hourglass network [51].

The other set of relevant works includes semi-supervised learning for segmentation. Recent works have explored adversarial training [20], student-teacher frameworks [9, 49] and self-training [64, 65]. Pseudo labelling is also explored in conjunction with augmentation techniques [45, 66]. In this work, we exploit the 2D-3D keypoint estimates to enhance the segmentation quality of pseudo labels as well as improving the 2D-3D keypoint estimates using the said segmentation pseudo-labels.

3. Keypoints and Planar Hulls for Weak and Semi-Supervision

Our task is to extract 3D structures in the form of 3D keypoints, given only an image of an object. This task has been explored before in the NrSfM settings. The existing methods rely on a large dataset with a weak-supervision of 2D keypoint annotations [34, 37, 54] by means of the projection consistency. However, collecting these annotations is time and effort consuming which limits the scaling of the existing methods to new objects and domains.

We present a framework that utilizes only a small amount of 2D labelled samples to produce competitive results com-

pared to fully supervised approaches. Our method relies on the proposed piece-wise planar hulls prior, which is defined for all objects of interest. The planar hulls prior is defined directly on the shape template, which is later used to derive the semantic regions on the images. The derived semantics serve as an additional supervisory signal while maintaining their consistency to the corresponding keypoints during the learning process. It is important to note that the planar hulls prior of the objects can be obtained simply by planar separation of the shape templates solely from the keypoint semantics, which is only required once per category.

Our weak and semi-supervised learning exploits, (i) partial labels of 2D keypoints for weak supervision using the labelled data, and (ii) cross-consistency between keypoints and planar hulls for self-supervision using the unlabelled data. For the latter, we derive the pseudo-labels using the proposed 2D pseudo-target and segmentation pseudo-label generation modules, as shown in Figure 1.

3.1. Preliminaries - NrSfM

In the NrSfM setting, an object is represented with a set of predefined keypoints. Given the 2D projections of these keypoints in n views of the object, the goal is estimating the 3D locations of the keypoints in all these views. Let $\mathbf{Y}_i = [\mathbf{y}_{i1}, \dots, \mathbf{y}_{ik}] \in \mathbb{R}^{2 \times k}$ be a stacked matrix representation of k 2D keypoints from the i^{th} view. The structure of the object at the i^{th} view is $\mathbf{X}_i = \alpha_i^\top \mathbf{B}$, with the shape basis $\mathbf{S} \in \mathbb{R}^{d \times 3k}$ and coefficients $\alpha_i \in \mathbb{R}^d$. We assume that the keypoints are centered and normalized and the camera follows an orthographic projection model, i.e. $\Pi = [\mathbf{I}_{2 \times 2} \ \mathbf{0}]$. Given the camera rotation matrix $\mathbf{R}_i \in \mathbf{SO}(3)$, as well as the centered and normalized keypoints, we can write $\mathbf{Y}_i = \Pi \mathbf{R}_i (\mathbb{I}_3 \odot \alpha_i^\top \mathbf{B})$, where the operation $\mathbb{I}_3 \odot \mathbf{b}$ reshapes the row vector $\mathbf{b} \in \mathbb{R}^{1 \times 3k}$ to a matrix of the from $\mathbb{R}^{3 \times k}$. In order to recover shape and pose a loss function is minimized:

$$\min_{\alpha_i, \mathbf{B}, \mathbf{R}_i \in \mathbf{SO}(3)} \sum_{i=1}^n \mathcal{L}(\mathbf{Y}_i, \Pi \mathbf{R}_i (\mathbb{I}_3 \odot \alpha_i^\top \mathbf{B})). \quad (1)$$

where $\mathcal{L}(a, b)$ is a norm-based loss of the form $\|a - b\|$. In the context of multi-class NrSfM, our method extracts 3D structures of objects from a wide variety of classes. Thus, $(\mathbb{I}_3 \odot \alpha_i^\top \mathbf{B}) \in \mathbb{R}^{3 \times k}$, should be able to express the 3D structure of objects with different number of keypoints. Let \mathbf{Z} represent the set of object categories and $z_i \in \mathbf{Z}$ be the category of sample i . Let each category $z \in \mathbf{Z}$ be represented by k_z keypoints, thus we have a total of $k = \sum_z k_z$ keypoints. To “access” the correct keypoints we have a subset selection vector $\zeta_z \in \{0, 1\}^k$ that indicates which dimensions relate to category z . Given these multi-category definitions, we

can reformulate (1) as

$$\min_{\alpha_i, \mathbf{B}, \mathbf{R}_i \in \mathbf{SO}(3)} \sum_{i=1}^n \mathcal{L}(\mathbf{Y}_i \circ \zeta_{z_i}, \Pi \mathbf{R}_i (\alpha_i^\top \mathbf{B}) \circ \zeta_{z_i}), \quad (2)$$

where \circ is the broadcasted elementwise multiplication. In this work, we use a deep learning approach and obtain α , \mathbf{B} and \mathbf{R} as outputs of a neural network. Thus, we will refer to $\mathbf{R}(\alpha^\top \mathbf{B})$ simply by $\hat{\mathbf{X}}$, which is the 3D shape in the camera coordinate frame.

3.2. Motivation

In our setting, we are given N_L images with ground truth 2D keypoint annotations and N_U images without annotations. We refer to the labelled and unlabelled samples as D_L D_U , respectively. Furthermore, the true 2D targets are denoted by $\bar{\mathbf{Y}}_{D_L}$. Recall that we aim to predict 3D keypoints directly from images. Let the 3D estimates of labelled samples be $\hat{\mathbf{X}}_{D_L}$ and the unlabelled samples be $\hat{\mathbf{X}}_{D_U}$. Building on (2), the most straightforward way to utilize unlabelled samples is to expand (2) in terms of the labelled and the unlabelled samples:

$$\min_{\alpha, \mathbf{B}, \mathbf{R}} \sum_{i=1}^{N_L} \mathcal{L}(\bar{\mathbf{Y}}_{D_L}^i, \Pi \hat{\mathbf{X}}_{D_L}^i) + \sum_{i=1}^{N_U} \mathcal{L}(\bar{\mathbf{Y}}_{D_U}^i, \Pi \hat{\mathbf{X}}_{D_U}^i), \quad (3)$$

where we drop $\circ \zeta_{z_i}$ for simplicity. The key problem of semi-supervised learning is that we do not have access to the true labels $\bar{\mathbf{Y}}_{D_U}$ for supervision. Therefore, we seek 2D pseudo-targets, say $\bar{\mathbf{Y}}_{D_U}$, instead. In this process we propose to perform an auxiliary task of semantic planar hulls prediction, which in turn will allow us to derive the required pseudo-labels. However, deriving these pseudo-labels which are effective for self-supervision is not trivial.

Our learning model takes an image as input and outputs (i) a segmentation map, (ii) 2D keypoint locations, and (iii) the corresponding 3D locations of the keypoints. Let us denote this model with $T(\mathcal{I}) = (\mathbf{S}, \mathbf{Y}, \mathbf{X})$ where $\mathcal{I} \in \mathbb{R}^{H \times W \times 3}$ is the image, $\mathbf{S} \in \mathbb{R}^{H \times W \times s}$ are the logits of the segmentation mask, $\mathbf{Y} \in \mathbb{R}^{k \times 2}$ are 2D keypoint locations, and $\mathbf{X} \in \mathbb{R}^{k \times 3}$ are the 3D locations of the keypoints. The segmentation branch in the proposed network learns to segment the components of 2D projections of the 3D piecewise planar hulls. The segmentation estimates are used in conjunction with the 2D and 3D keypoint estimates to obtain pseudo-labels $\hat{\mathbf{Y}}_{D_L}$. This allows us to leverage the unlabelled data, in a self-supervised fashion, for the semi-supervised learning.

3.3. Piecewise Planar Hulls

We propose a new labelling structure on top of the traditional 2D keypoints. We propose the Piecewise Planar Hull (PPH) which is a simple list of semantically meaningful keypoint cliques. Each entry in this list encodes a plane in terms

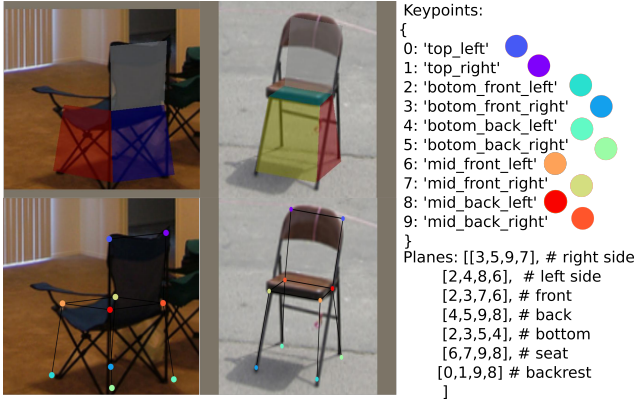


Figure 2. PPH of chair class. The planes are chosen to enclose the smallest 3D hull of the keypoints while considering the semantics of the keypoints.

of the keypoints. The union of these planes form the 3D hull that encloses all the keypoints. Since the planes are defined by the semantics, the PPH only needs to be defined once for a category and takes a few seconds to create, see Figure 3. It is possible to define PPH in different ways for a category, however, (i) each point has to appear in at least one plane and (ii) no two planes should intersect except possibly along their shared edges. Note that in this sentence intersection in 3D is meant and their 2D projections are of course allowed to overlap. The PPHs should ideally be defined such that each plane corresponds to a clear semantically distinguishable surface. This is important for the performance of the semantic segmentation network. For most object classes, this is naturally satisfied since the keypoints are semantically meaningful to begin with. For most categories, the choice of the planes are somewhat determined by the semantics of the defined keypoints. In our selection, apart from the semantics, we chose configurations that minimize the 3D volume the hull occupies. Note that, the planes do not need to correspond to a real surface and can simply be the region between semantically relevant keypoints, where an example is given in Fig.8.

Another important aspect is the symmetric planes. For example, left and right sides of the car are symmetric and if only the surfaces are considered identical. However, the methods can identify the left and right through referencing on the unique planes such as the front window of the car. In order to facilitate this, we use Coordinate convolutions CoordConv [28]. CoordConv creates a grid of 2D locations and concatenate this grid with the input feature map. The convolution operation is then applied on this concatenated representation. In our setting, this is important to enable the model have a geometric and spatial reasoning. Please refer to Supp for an extended discussion.

PPH can be used to produce a segmentation mask for a

given sample. Given the 2D keypoint locations it is possible to extract each plane. In order to form the segmentation mask, visibility of each plane should be determined. For the labelled samples, visibility of the planes can easily be extracted from the visibility of the keypoints, which is supplied in the dataset. For the unlabelled samples, we use the network estimates to determine visibility, as explained in the next Section. Overall, each sample provides the following information for each plane P_i in PPH: 2D and 3D locations of the vertices P_Y^i and P_X^i , respectively, as well as the “visibility” indicator $P_V^i \in \{0, 1\}$. By using the pre-defined planar surfaces, it is possible to train a segmentation network with a fixed number of classes, i.e. the number of planes. Let the number of planes for the object category z be s_z , then the total number of segmentation classes $s = \sum_z s_z + 1$ with the shared background class.

3.4. Cross Consistency between Keypoints and Planar Hulls

To leverage the unlabeled data, we exploit the cross consistency prior between keypoints and planar hulls’ semantics. This is done by iteratively deriving segmentation pseudo-labels \bar{S}_{DU} and 2D keypoint pseudo-targets \bar{Y}_{DU} from the network’s predictions. We propose two modules: (i) 2D pseudo-target generation, (ii) semantic pseudo-label generation. The generated pseudo-labels are used to supervise the respective branches of the network, using the unlabeled data. For labeled data, we use 2D, segmentation, and reprojection losses with ground truth.

4. Pseudo-label Generation and Semi-supervised Learning

4.1. Semantic Pseudo-label Generation

Let us assume the network T is trained with the labelled samples. The segmentation mask branch is trained by the ground truth planes, which are solely extracted from the true keypoint locations. The 2D keypoint branch is trained with the given true keypoints and the 3D branch is trained through minimizing the reprojection error. Thus, the whole network is trained only using 2D annotations.

As discussed, to utilize the unlabelled samples, we use pseudo-labelling on the segmentation masks. Specifically, a given pixel location in the pseudo-label can take one of $s + 1$ values, which represent the total number of planes plus the background class, i.e. s and the special class of ‘uncertain’. If a pixel is ‘certain’ the corresponding label is set to the class with the highest probability. The resulting estimated pseudo-label is denoted with L_E . Identifying the uncertain pixels and using only ‘certain’ pseudo-labels is a common technique in the semi-supervised setting. To do so, we produce the uncertainty measure through three mechanisms: Monte carlo dropout, visibility, and plane agreement.



Figure 3. Piecewise Planar Hull mapping for the category car, illustrating the semantic meaning. Under each sample the visibility of each plane (P_V) is also given. PPH is defined once per category and visibility information P_V is extracted from the keypoint labels and the estimates.

We produce segmentation pseudo-labels offline after some number of epochs of training. Each time, new pseudo-labels are generated, we enter a new **recursion**.

Monte Carlo Dropout: Monte Carlo dropout is a well established measure of uncertainty [16]. We add dropout layers in the segmentation branch of T and in the pseudo-labelling step, we run the network N_D times with dropout probability of p_D at all layers. This process results in a logits matrix R_D of dimensions $N_D \times H \times W \times s$. We use Welch’s t -test per pixel on the logits distribution of the two most probable classes. Specifically, let the most probable class for a pixel location $u = (h, w) \in [1, H] \times [1, W]$ be $M_u = \arg \max_s \text{mean}_{N_D}(\text{softmax}_s(R_D[u]))$ and similarly, the second most probable class $N_u = \arg \max_{s, s \neq M_u} \text{mean}_{N_D}(\text{softmax}_s(R_D[u]))$. Then, $V_M^u, V_N^u \in \mathbb{R}^{N_D}$ represent the logits vector for classes M_u and N_u . We treat these vectors as samples from two distributions and conclude that the pixel u is ‘uncertain’ if t -test probability $p \geq 0.05$. Here, p represents the probability that two sets of samples are from distributions with the same mean.

Visibility: The 3D keypoint estimated by the network are used to establish the plane visibility. In other words, it is possible to estimate the P_V indicator of the estimated planes. In order to achieve this, all planes are formed in 3D. A plane is occluded if more than half of its 2D projected area remains behind other planes. The pixels in the pseudo-label that belong to the occluded planes are set to “uncertain”. Furthermore, the 3D estimates can also have depth ambiguity. Thus, the visibility estimations are prone to error. To alleviate this problem, we calculate visibility with the current and the reversed depth values. Then, we pick the direction with the highest agreement with the segmentation estimates.

Plane Estimation Agreement: 2D estimates of the network are used to create planes. The set of planes with the selected depth direction is used for calculations. The plane estimates

are compared against the segmentation estimate and the non-intersecting pixels are set to ‘uncertain’.

4.2. 2D Pseudo-target Generation

With segmentation pseudo-labels, the network can be trained to estimate 2D keypoints such that the resulting planar map maximizes the Intersection-Over-Union (IOU) with respect to pseudo-labels, see Figure 4. However, converting segmentation pseudo-labels into 2D keypoint locations is not trivial. In order to achieve this, we first attempt to obtain the planes with the highest IOU with the segmentation pseudo-labels. Then, we extract keypoint locations as the vertices of the “best fitting” planes. In this process, we use the exploration-exploitation scheme. Given the 2D keypoint estimates \mathbf{Y} and 3D location estimates \mathbf{X} , we produce n_Q planar maps by adding Gaussian noise on the x-y locations of the 2D keypoint estimates and using the depth given by $\hat{\mathbf{X}}$.

In order to alleviate the depth ambiguity problem, we first select the correct depth direction of \mathbf{X} with the aforementioned procedure in “visibility reasoning”. We avoid adding noise to the depth values for computational efficiency. Let the resulting set of planar maps be M_Q . Furthermore, we also generate the planar map dictated by the current estimates \mathbf{Y} , which we refer to as the **reference map** M_R . This process results in $N_R + 1$ planar maps with $s_z \times (n_Q + 1)$ planes where z represents the class of the object. Altogether, the resulting planar maps are denoted by M_T .

Given that one keypoint can appear in multiple planes, we do not need to fit all the planes accurately. Thus, we use only a subset of the $s_z \times (n_Q + 1)$ planes such that the keypoints are estimated through using more accurate planes. Therefore, we select one plane for each keypoint. Note that the same plane can be chosen for multiple keypoints. Let us denote the selected plane for the keypoint i be P_i .

Then, the desired P_i is the one that maximizes the IOU

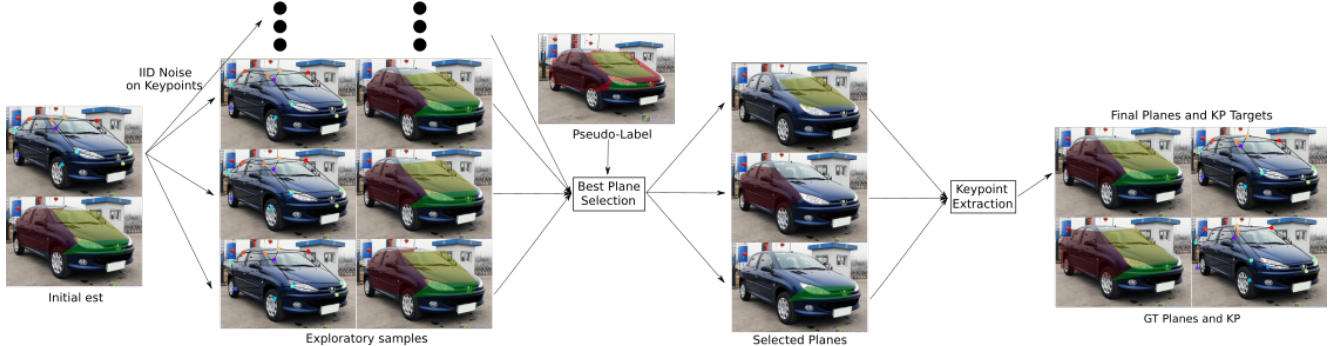


Figure 4. 2D pseudo-target generation pipeline. We generate 2D keypoint targets through randomly re-sampling them nearby and then choosing the planes that have highest IOU with the pseudo-labels.

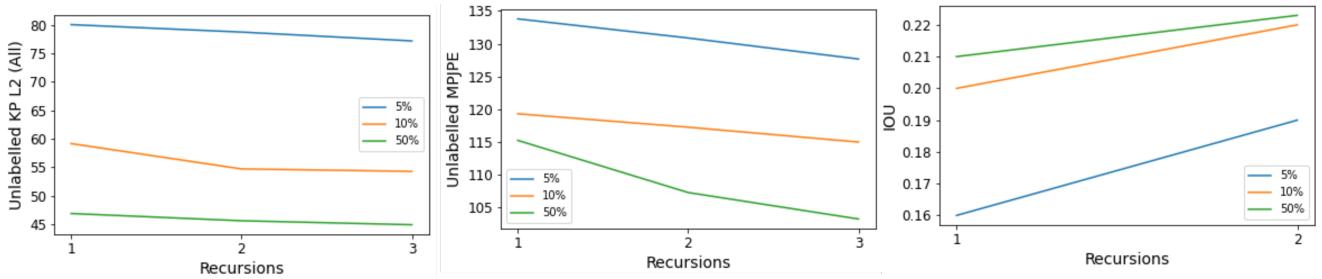


Figure 5. The 2D keypoint, 3D MPJPE and mIOU segmentation results on the unlabelled training samples. The proposed framework clearly improves the accuracy on unlabelled samples.

with its corresponding pseudo-label. We implement this *argmax* operation as a two-step procedure. First, for each keypoint i , the set of planes in the reference map that includes the keypoint i are extracted. Among these planes, the one with the highest IOU with its pseudo-label is chosen. In mathematical terms,

$$\hat{P}_i = \arg \max_{p \in M_R, i \in p} \text{IOU}(p, L_E^p), \quad (4)$$

where L_E^p denotes the binary mask belonging to the region of the pseudo-label with class p . \hat{P}_i indicates which predefined planar structure that includes the keypoint i , currently captures the segmentation estimates best. This operation corresponds to selecting a planar class from s_z options. Thus, given \hat{P}_i , we can select the corresponding $N_R + 1$ planes among $s_z \times (N_R + 1)$ candidates. Note that, it is possible that there is no visible plane or ‘certain’ pseudo-label class that a given keypoint belongs to. If this is the case, $\hat{P}_i = \emptyset$. At this point, if $\hat{P}_i \neq \emptyset$, the desired plane is given by,

$$P_i = \arg \max_{p \in M_T(\hat{P}_i)} \text{IOU}(p, L_E^p), \quad (5)$$

where $M_T(\hat{P}_i)$ selects the set of planes indicated by \hat{P}_i among the planes induced by M_T . Since M_R is included in M_T , this process can result in the selection of a plane estimated by the network.

In order to generate the target 2D keypoint locations, we first obtain the set union of all the best planes P_i , resulting in the set of planes P_U . The 2D target of a keypoint i , $\bar{Y}_{D_U}[i]$ is then given by the mean of the locations of the corresponding vertices of all the planes in P_U . More precisely,

$$\bar{Y}_{D_U}[i] = \begin{cases} \mathbf{Y}_i & P_i = \emptyset \\ \text{mean}_{j,i \in P_j, P_j \in P_U}(P_j(i)) & P_i \neq \emptyset. \end{cases} \quad (6)$$

Note that when the network’s estimate is better than the ‘exploratory’ options, no penalty is incurred.

4.3. The Network Training Scheme

In order to fully utilize the labelled and unlabelled data, the network T is trained using both types of data at each iteration. Let us rewrite the network $T(\mathcal{I}) = (\mathbf{S}, \mathbf{Y}, \mathbf{X})$ as composition of several sub-networks. Specifically,

$$\begin{aligned} \hat{\mathbf{S}} &= T_S(T_B(\mathcal{I})), \\ \hat{\mathbf{Y}} &= T_Y(T_R(T_B(\mathcal{I}))), \\ \hat{\mathbf{X}} &= T_X(T_R(T_B(\mathcal{I})), \hat{\mathbf{Y}}) \end{aligned} \quad (7)$$

where $T_B(\mathcal{I})$ represents the backbone network that produces feature maps from the image and $T_R(\cdot)$ is a sub-network that produces further feature vectors that are used for the 2D and 3D keypoint estimations. Note that 3D keypoint locations directly depend on the 2D keypoint locations.

The hat operator $\hat{\cdot}$ indicates that the given variable is estimated by the network.

Let us denote the true segmentation maps and 2D keypoint locations for the labelled samples by $\bar{\mathbf{S}}_{D_L}, \bar{\mathbf{Y}}_{D_L}$. Furthermore, for the unlabelled samples let us refer to the segmentation pseudo-labels by $\bar{\mathbf{S}}_{D_U}$ and the 2D keypoint targets found by fitting to the best plane, by $\bar{\mathbf{Y}}_{D_U}$. Resulting in the losses:

- 2D loss $\mathcal{L}_{2D}^{D_L} = \|\bar{\mathbf{Y}}_{D_L} - \hat{\mathbf{Y}}_{D_L}\|_1$,
 $\mathcal{L}_{2D}^{D_U} = \|\bar{\mathbf{Y}}_{D_U} - \hat{\mathbf{Y}}_{D_U}\|_1$
- Segmentation loss $\mathcal{L}_S^{D_L} = \mathcal{L}_{CE}(\bar{\mathbf{S}}_{D_L}, \hat{\mathbf{S}}_{D_L})$,
 $\mathcal{L}_S^{D_U} = \mathcal{L}_{CE}(\bar{\mathbf{S}}_{D_U}, \hat{\mathbf{S}}_{D_U})$
- Reprojection loss $\mathcal{L}_R^{D_L} = \mathcal{L}_H(\hat{\mathbf{Y}}_{D_L}, \Pi \hat{\mathbf{X}}_{D_L})$,
 $\mathcal{L}_R^{D_U} = \mathcal{L}_H(\hat{\mathbf{Y}}_{D_U}, \Pi \hat{\mathbf{X}}_{D_U})$

where \mathcal{L}_{CE} is the pixelwise cross-entropy loss, \mathcal{L}_H the Huber loss and Π the orthographic projection operator. For the segmentation loss of unlabelled samples, $\mathcal{L}_S^{D_U}$, only the “certain” pixels are considered. For the total loss, the terms are combined using hyperparameters. Note that, the whole proposed pipeline is generic and can be implemented with any particular architecture.

5. Network Architecture

We propose a baseline architecture for the proposed generic framework. The network T should be able to produce segmentation masks, 2D keypoints and their 3D locations from only an image for a wide variety of object classes. Moreover, the architecture is designed in such a way that new object classes can be added easily without training a new network from scratch. Among the sub-networks mentioned in (7), T_Y is an MLP that maps the input feature vectors to 2D coordinates. For the backbone T_B , we use an Imagenet pre-trained Resnet. The segmentation subnetwork T_S is a simple decoder with residual blocks [18] and bilinear upsampling, see Supp for details. While it is possible to improve the performance of the segmentation network with more sophisticated architectures, we opt for a simple design that will suffice to demonstrate the effectiveness of the proposed framework. For the 2D-3D network T_X , we use the same architecture as [34].

Finally, the network T_R should produce keypoints from the given image. For this network, we opt for a DETR [5] based architecture, since it can be finetuned if further objects are added. Each object class has a pre-determined number of keypoints. Thus each keypoint is represented with a learnt query vector. This means there are $k = \sum_z k_z$, see 3.1, query vectors where z iterates over the object classes. These query vectors are processed jointly by the transformer to obtain k feature vectors. Note that all k query vectors are processed, independent of the object class. Then, the feature

vectors corresponding to the class of the object are processed further by T_Y to obtain the 2D locations.

6. Experiments

We experiment on the **PASCAL3D+** dataset since it is the only benchmark dataset with variety of categories. We use the pre-processed version of [34]. There are only a few NrSfM methods that can handle a setting as diverse as our method. We compare against C3DPO [35], EMSfM [50], GbNrSfM [15] and CMR [22]. Some methods in the literature report results on Pascal3D by using GT keypoints but they refrain from reporting their results with estimated keypoints [15, 50, 54]. We report absolute mean per joint position error $\text{MPJPE}(X, Y) = \sum_{k=1}^K \|X_k - Y_k\|/K$ and $\text{Stress}(X, Y) = \sum_{i < j} \|(X_i - X_j) - (Y_i - Y_j)\|_1/(K(K-1))$. We follow the same train/test split and evaluation procedure as [35].

Implementation. We use a dropout probability of 0.2 at each segmentation network layer and use 50 Monte-Carlo runs. At 2D Pseudo-target generation step, the Gaussian noise std is set to 0.01. We freeze the backbone for semi-supervised networks and fine-tuned for the “100% data utilization model”. Moreover, “100% data utilization model” does not have a segmentation branch.

7. Results

We give some quantitative and qualitative results to show the effectiveness of the proposed framework, where more results can be found in Supp. In Table 1, we present the test results of SOTA methods as well as Ours. It can be seen that, even though other methods use pretrained stacked hourglass (SH) networks, our semi-supervised results outperform all other semi-supervised approaches. By using only 50% of the data, our method produces comparable results to fully-supervised competitors. Moreover, our fully-supervised approach produces the best results. Table 2 shows the 2D keypoint performance compared to SH networks. It can be seen that our method outperforms SH on all keypoints while SH is performing better in estimating the visible keypoints.

We present the performance of our method on the test set at different recursions in Figure 6. The results show that the performance improves with recursions. This also confirms the effectiveness of the proposed framework.

Apart from the performance on the test set, we also present the performance of the proposed framework on the unlabelled samples of the training set in Figure 5. The results show that 2D keypoint estimates, segmentation estimates and 3D estimates all get better. This validates that the proposed framework results in better pseudo-labels for the unlabelled samples.

The visual results are given in Figure 7 where it can be clearly seen that the proposed method improves the results

Method	EMSfM*	GbSfM*	CMR/SH†	C3DPO/SH†				Ours			
Train Data %	100	100	100	5	10	50	100	5	10	50	100
MPJPE	131.0	184.6	74.4	86.3	79.6	77.2	57.4	85.6	76.3	68.7	51.6
Stress	116.8	111.3	53.7	70.1	64.8	59.2	41.4	54.8	52.5	50.9	35.3

Table 1. Results on Pascal3D. †: 2D keypoint estimator stacked hourglass network is pretrained and further trained using 100% of training data. * Method uses GT 2D keypoints at test time.

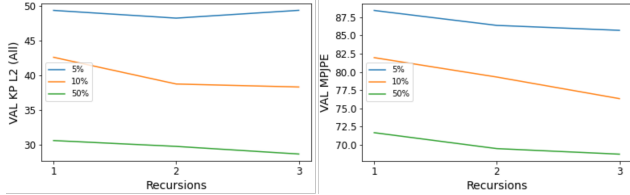


Figure 6. The 2D keypoint estimation L2 distance and 3D MPJPE on test set for different recursions.

Method	SH	Ours				
		Train %	100	5	10	50
L2 (All KP)	35.6	49.4	38.3	28.9	28.2	
L2 (Vis KP)	18.6	48.1	37.1	27.3	26.5	

Table 2. 2D keypoint estimations on Pascal3D for all defined (All KP) and the visible keypoints (Vis KP).

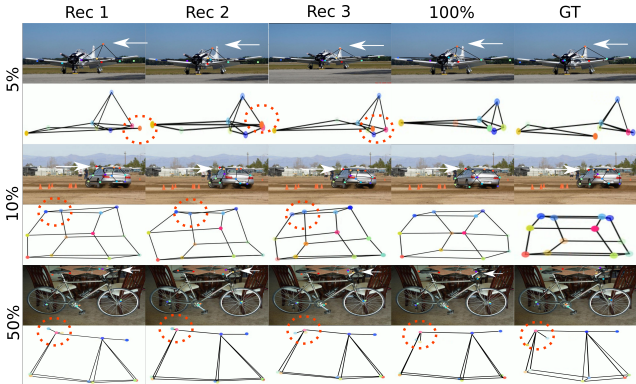


Figure 7. Test results for models trained with different annotation ratios at different recursions. The results become more accurate over recursion. Points of interest are marked with red circles and arrows. The improvements in overall locations of the plane, in the corner of the car and the handlebar of the bike both in 2D and 3D are significant.

at every recursion. Moreover, even with 5% training data, the network can estimate accurate 3D shapes.

7.1. Ablation

A natural question to ask is the dependence of the framework on the different definitions of the PPHs. While for

most closed convex objects such as cars, bus, sofa etc. the definition is somewhat ubiquitous, for some other categories like bicycle and airplane, the definitions mostly depend on the annotator. Here we present our results when the PPH definitions of bicycle and airplane are different than the ones we used in the paper, see Supp for details. In Table 4, we present the 3D results of the ablated version with an asterisk. It can be seen that the results are very similar to each other on average. This shows that the performance of the framework does not depend on the PPH definitions very much.

Method	Ours				Ours*			
	Train Data %	5	10	50	100	5	10	50
MPJPE	85.6	76.3	68.7	51.6	85.5	75.1	68.9	
Stress	54.8	52.5	50.9	35.3	55.3	51.0	51.3	

Table 3. Results on Pascal3D with bicycle and airplane classes for different PPH definitions.

8. Conclusion

We proposed a semi-supervision framework for 3D shape and pose estimation in terms of keypoints. In this framework, a model is trained with limited 2D keypoint annotations, which at test time can estimate the 3D shape and pose directly from a single image. To achieve this, we propose *piecewise planar hulls* which are structures that form a bridge between semantic segmentation and keypoint estimation. This relationship allowed us to derive the self-supervision loss, thereby enabling us to efficiently use unlabelled data. The proposed self-supervision relies on the pseudo-labels derived from the predictions and the cross-consistency between them. In this work, we also presented an exploration-exploitation technique to effectively generate pseudo-targets for 2D keypoints from segmentation pseudo-labels using piecewise planar hulls. The experiments show that the proposed framework consistently offers very promising results compared to the baseline and the state-of-the-art methods. In the semi-supervised setting, it achieves comparable results with fully supervised state-of-the-art methods by using only half of the annotations.

Limitations. The online 2D Pseudo-target generation process is slow and increases the training time. This inhibits training longer and effects the performance negatively.

References

- [1] Ijaz Akhter, Yaser Sheikh, Sohaib Khan, and Takeo Kanade. Trajectory space: A dual representation for nonrigid structure from motion. *IEEE Trans. Pattern Anal. Mach. Intell.*, 33(7):1442–1456, 2011.
- [2] Adrien Bartoli, Vincent Gay-Bellile, Umberto Castellani, Julien Peyras, Søren I. Olsen, and Patrick Sayd. Coarse-to-fine low-rank structure-from-motion. In *2008 IEEE Computer Society Conference on Computer Vision and Pattern Recognition (CVPR 2008), 24-26 June 2008, Anchorage, Alaska, USA*. IEEE Computer Society, 2008.
- [3] Federica Bogo, Angjoo Kanazawa, Christoph Lassner, Peter Gehler, Javier Romero, and Michael J Black. Keep it smpl: Automatic estimation of 3d human pose and shape from a single image. In *European Conference on Computer Vision*, pages 561–578. Springer, 2016.
- [4] Zhe Cao, Tomas Simon, Shih-En Wei, and Yaser Sheikh. Realtime multi-person 2d pose estimation using part affinity fields. In *Proceedings of the IEEE Conference on Computer Vision and Pattern Recognition*, pages 7291–7299, 2017.
- [5] Nicolas Carion, Francisco Massa, Gabriel Synnaeve, Nicolas Usunier, Alexander Kirillov, and Sergey Zagoruyko. End-to-end object detection with transformers. In Andrea Vedaldi, Horst Bischof, Thomas Brox, and Jan-Michael Frahm, editors, *Computer Vision - ECCV 2020 - 16th European Conference, Glasgow, UK, August 23-28, 2020, Proceedings, Part I*, volume 12346 of *Lecture Notes in Computer Science*, pages 213–229. Springer, 2020.
- [6] Geonho Cha, Minsik Lee, and Songhwai Oh. Unsupervised 3d reconstruction networks. In *2019 IEEE/CVF International Conference on Computer Vision, ICCV 2019, Seoul, Korea (South), October 27 - November 2, 2019*, pages 3848–3857. IEEE, 2019.
- [7] Ching-Hang Chen, Ambrish Tyagi, Amit Agrawal, Dylan Drover, Rohith MV, Stefan Stojanov, and James M. Rehg. Unsupervised 3d pose estimation with geometric self-supervision. In *IEEE Conference on Computer Vision and Pattern Recognition, CVPR 2019, Long Beach, CA, USA, June 16-20, 2019*, pages 5714–5724. Computer Vision Foundation / IEEE, 2019.
- [8] Liang-Chieh Chen, Raphael Gontijo Lopes, Bowen Cheng, Maxwell D. Collins, Ekin D. Cubuk, Barret Zoph, Hartwig Adam, and Jonathon Shlens. Naive-student: Leveraging semi-supervised learning in video sequences for urban scene segmentation. In Andrea Vedaldi, Horst Bischof, Thomas Brox, and Jan-Michael Frahm, editors, *Computer Vision - ECCV 2020 - 16th European Conference, Glasgow, UK, August 23-28, 2020, Proceedings, Part IX*, volume 12354 of *Lecture Notes in Computer Science*, pages 695–714. Springer, 2020.
- [9] Xiaokang Chen, Yuhui Yuan, Gang Zeng, and Jingdong Wang. Semi-supervised semantic segmentation with cross pseudo supervision. In *Proceedings of the IEEE/CVF Conference on Computer Vision and Pattern Recognition*, pages 2613–2622, 2021.
- [10] Yuchao Dai, Hongdong Li, and Mingyi He. A simple prior-free method for non-rigid structure-from-motion factorization. *Int. J. Comput. Vis.*, 107(2):101–122, 2014.
- [11] Zheng Dang, Fei Wang, and Mathieu Salzmann. 3d registration for self-occluded objects in context. *arXiv preprint arXiv:2011.11260*, 2020.
- [12] Ingrid Daubechies, Michel Defrise, and Christine De Mol. An iterative thresholding algorithm for linear inverse problems with a sparsity constraint. *Communications on Pure and Applied Mathematics: A Journal Issued by the Courant Institute of Mathematical Sciences*, 57(11):1413–1457, 2004.
- [13] Zhengyang Feng, Qianyu Zhou, Guangliang Cheng, Xin Tan, Jianping Shi, and Lizhuang Ma. Semi-supervised semantic segmentation via dynamic self-training and class-balanced curriculum. *CoRR*, abs/2004.08514, 2020.
- [14] Clara Fernandez-Labrador. *Indoor Scene Understanding using Non-Conventional Cameras*. PhD thesis, Université de Bourgogne Franche-Comté (COMUE)(UBFC), FRA.; Universidad . . ., 2020.
- [15] Katerina Fragkiadaki, Marta Salas, Pablo Andrés Arbeláez, and Jitendra Malik. Grouping-based low-rank trajectory completion and 3d reconstruction. In Zoubin Ghahramani, Max Welling, Corinna Cortes, Neil D. Lawrence, and Kilian Q. Weinberger, editors, *Advances in Neural Information Processing Systems 27: Annual Conference on Neural Information Processing Systems 2014, December 8-13 2014, Montreal, Quebec, Canada*, pages 55–63, 2014.
- [16] Yarin Gal and Zoubin Ghahramani. Dropout as a bayesian approximation: Representing model uncertainty in deep learning. In *international conference on machine learning*, pages 1050–1059. PMLR, 2016.
- [17] Kaiming He, Georgia Gkioxari, Piotr Dollár, and Ross Girshick. Mask r-cnn. In *Proceedings of the IEEE international conference on computer vision*, pages 2961–2969, 2017.
- [18] Kaiming He, Xiangyu Zhang, Shaoqing Ren, and Jian Sun. Deep residual learning for image recognition. In *2016 IEEE Conference on Computer Vision and Pattern Recognition, CVPR 2016, Las Vegas, NV, USA, June 27-30, 2016*, pages 770–778. IEEE Computer Society, 2016.
- [19] Yisheng He, Yao Wang, Haoqiang Fan, Jian Sun, and Qifeng Chen. FS6D: few-shot 6d pose estimation of novel objects. *CoRR*, abs/2203.14628, 2022.
- [20] Wei-Chih Hung, Yi-Hsuan Tsai, Yan-Ting Liou, Yen-Yu Lin, and Ming-Hsuan Yang. Adversarial learning for semi-supervised semantic segmentation. *arXiv preprint arXiv:1802.07934*, 2018.
- [21] Simon Jenni and Paolo Favaro. Self-supervised multi-view synchronization learning for 3d pose estimation. In Hiroshi Ishikawa, Cheng-Lin Liu, Tomás Pajdla, and Jianbo Shi, editors, *Computer Vision - ACCV 2020 - 15th Asian Conference on Computer Vision, Kyoto, Japan, November 30 - December 4, 2020, Revised Selected Papers, Part V*, volume 12626 of *Lecture Notes in Computer Science*, pages 170–187. Springer, 2020.
- [22] Angjoo Kanazawa, Shubham Tulsiani, Alexei A. Efros, and Jitendra Malik. Learning category-specific mesh reconstruction from image collections. In Vittorio Ferrari, Martial Hebert, Cristian Sminchisescu, and Yair Weiss, editors, *Computer Vision - ECCV 2018 - 15th European Conference, Munich, Germany, September 8-14, 2018, Proceedings, Part XV*, vol-

- ume 11219 of *Lecture Notes in Computer Science*, pages 386–402. Springer, 2018.
- [23] Laurent Kneip, Hongdong Li, and Yongduek Seo. Upnp: An optimal $O(n)$ solution to the absolute pose problem with universal applicability. In David Fleet, Tomas Pajdla, Bernt Schiele, and Tinne Tuytelaars, editors, *Computer Vision – ECCV 2014: 13th European Conference, Zurich, Switzerland, September 6–12, 2014, Proceedings, Part I*, 2014.
- [24] Filippos Kokkinos and Iasonas Kokkinos. To the point: Correspondence-driven monocular 3d category reconstruction. *CoRR*, abs/2106.05662, 2021.
- [25] Chen Kong and Simon Lucey. Prior-less compressible structure from motion. In *2016 IEEE Conference on Computer Vision and Pattern Recognition, CVPR 2016, Las Vegas, NV, USA, June 27–30, 2016*, pages 4123–4131. IEEE Computer Society, 2016.
- [26] Chen Kong and Simon Lucey. Deep non-rigid structure from motion. In *2019 IEEE/CVF International Conference on Computer Vision, ICCV 2019, Seoul, Korea (South), October 27 - November 2, 2019*, pages 1558–1567. IEEE, 2019.
- [27] Chen Kong, Rui Zhu, Hamed Kiani, and Simon Lucey. Structure from category: A generic and prior-less approach. In *Fourth International Conference on 3D Vision, 3DV 2016, Stanford, CA, USA, October 25–28, 2016*, pages 296–304. IEEE Computer Society, 2016.
- [28] Rosanne Liu, Joel Lehman, Piero Molino, Felipe Petroski Such, Eric Frank, Alex Sergeev, and Jason Yosinski. An intriguing failing of convolutional neural networks and the coordinateconv solution. *Advances in neural information processing systems*, 31, 2018.
- [29] Matthew Loper, Naureen Mahmood, Javier Romero, Gerard Pons-Moll, and Michael J. Black. SMPL: A skinned multi-person linear model. *ACM Trans. Graphics (Proc. SIGGRAPH Asia)*, 34(6):248:1–248:16, 2015.
- [30] Q.-T. Luong and O.D. Faugeras. The fundamental matrix: theory, algorithms, and stability analysis. *International Journal of Computer Vision*, 17:43–75, 1995.
- [31] Eric Marchand, Hideaki Uchiyama, and Fabien Spindler. Pose estimation for augmented reality: a hands-on survey. *IEEE transactions on visualization and computer graphics*, 22(12):2633–2651, 2015.
- [32] Sudhanshu Mittal, Maxim Tatarchenko, and Thomas Brox. Semi-supervised semantic segmentation with high-and low-level consistency. *IEEE transactions on pattern analysis and machine intelligence*, 43(4):1369–1379, 2019.
- [33] Francesc Moreno-Noguer. 3d human pose estimation from a single image via distance matrix regression. In *Proceedings of the IEEE Conference on Computer Vision and Pattern Recognition*, pages 2823–2832, 2017.
- [34] David Novotny, Nikhila Ravi, Benjamin Graham, Natalia Neverova, and Andrea Vedaldi. C3dpo: Canonical 3d pose networks for non-rigid structure from motion. In *Proceedings of the IEEE International Conference on Computer Vision*, pages 7688–7697, 2019.
- [35] David Novotný, Nikhila Ravi, Benjamin Graham, Natalia Neverova, and Andrea Vedaldi. C3DPO: canonical 3d pose networks for non-rigid structure from motion. In *2019 IEEE/CVF International Conference on Computer Vision, ICCV 2019, Seoul, Korea (South), October 27 - November 2, 2019*, pages 7687–7696. IEEE, 2019.
- [36] Shaifali Parashar, Mathieu Salzmann, and Pascal Fua. Local non-rigid structure-from-motion from diffeomorphic mappings. In *2020 IEEE/CVF Conference on Computer Vision and Pattern Recognition, CVPR 2020, Seattle, WA, USA, June 13–19, 2020*, pages 2056–2064. Computer Vision Foundation / IEEE, 2020.
- [37] Sungheon Park, Minsik Lee, and Nojun Kwak. Procrustean regression: A flexible alignment-based framework for nonrigid structure estimation. *IEEE Transactions on Image Processing*, 27(1):249–264, 2017.
- [38] Sungheon Park, Minsik Lee, and Nojun Kwak. Procrustean regression: A flexible alignment-based framework for nonrigid structure estimation. *IEEE Trans. Image Process.*, 27(1):249–264, 2018.
- [39] Sungheon Park, Minsik Lee, and Nojun Kwak. Procrustean regression networks: Learning 3d structure of non-rigid objects from 2d annotations. In Andrea Vedaldi, Horst Bischof, Thomas Brox, and Jan-Michael Frahm, editors, *Computer Vision - ECCV 2020 - 16th European Conference, Glasgow, UK, August 23–28, 2020, Proceedings, Part XXIX*, volume 12374 of *Lecture Notes in Computer Science*, pages 1–18. Springer, 2020.
- [40] Mihir Sahasrabudhe, Zhixin Shu, Edward Bartrum, Riza Alp Güler, Dimitris Samaras, and Iasonas Kokkinos. Lifting autoencoders: Unsupervised learning of a fully-disentangled 3d morphable model using deep non-rigid structure from motion. In *2019 IEEE/CVF International Conference on Computer Vision Workshops, ICCV Workshops 2019, Seoul, Korea (South), October 27–28, 2019*, pages 4054–4064. IEEE, 2019.
- [41] Torsten Sattler, Bastian Leibe, and Leif Kobbelt. Fast image-based localization using direct 2d-to-3d matching. In *2011 International Conference on Computer Vision*, pages 667–674. IEEE, 2011.
- [42] Jingnan Shi, Heng Yang, and Luca Carlone. Optimal pose and shape estimation for category-level 3d object perception. *arXiv preprint arXiv:2104.08383*, 2021.
- [43] Jamie Shotton, Andrew Fitzgibbon, Mat Cook, Toby Sharp, Mark Finocchio, Richard Moore, Alex Kipman, and Andrew Blake. Real-time human pose recognition in parts from single depth images. In *CVPR 2011*, pages 1297–1304. Ieee, 2011.
- [44] N. Snavely, S. M. Seitz, and R. Szeliski. Modeling the world from internet photo collections. *Int. J. Comput. Vision*, 80(2):189–210, 2007.
- [45] Kihyuk Sohn, David Berthelot, Nicholas Carlini, Zizhao Zhang, Han Zhang, Colin A Raffel, Ekin Dogus Cubuk, Alexey Kurakin, and Chun-Liang Li. Fixmatch: Simplifying semi-supervised learning with consistency and confidence. *Advances in Neural Information Processing Systems*, 33:596–608, 2020.
- [46] Martin Sundermeyer, Zoltan-Csaba Marton, Maximilian Durner, and Rudolph Triebel. Augmented autoencoders: Implicit 3d orientation learning for 6d object detection. *International Journal of Computer Vision*, 128(3):714–729, 2020.
- [47] Supasorn Suwajanakorn, Noah Snavely, Jonathan Tompson, and Mohammad Norouzi. Discovery of latent 3d key-

- points via end-to-end geometric reasoning. *arXiv preprint arXiv:1807.03146*, 2018.
- [48] Hao Tang, Dan Xu, Gaowen Liu, Wei Wang, Nicu Sebe, and Yan Yan. Cycle in cycle generative adversarial networks for keypoint-guided image generation. In *Proceedings of the 27th ACM International Conference on Multimedia*, pages 2052–2060, 2019.
- [49] Antti Tarvainen and Harri Valpola. Mean teachers are better role models: Weight-averaged consistency targets improve semi-supervised deep learning results. *Advances in neural information processing systems*, 30, 2017.
- [50] Lorenzo Torresani, Aaron Hertzmann, and Christoph Bregler. Nonrigid structure-from-motion: Estimating shape and motion with hierarchical priors. *IEEE Trans. Pattern Anal. Mach. Intell.*, 30(5):878–892, 2008.
- [51] Alexander Toshev and Christian Szegedy. Deeppose: Human pose estimation via deep neural networks. In *2014 IEEE Conference on Computer Vision and Pattern Recognition, CVPR 2014, Columbus, OH, USA, June 23-28, 2014*, pages 1653–1660. IEEE Computer Society, 2014.
- [52] Shubham Tulsiani and Jitendra Malik. Viewpoints and keypoints. In *Proceedings of the IEEE Conference on Computer Vision and Pattern Recognition*, pages 1510–1519, 2015.
- [53] Angtian Wang, Shenxiao Mei, Alan L. Yuille, and Adam Kortylewski. Neural view synthesis and matching for semi-supervised few-shot learning of 3d pose. In Marc'Aurelio Ranzato, Alina Beygelzimer, Yann N. Dauphin, Percy Liang, and Jennifer Wortman Vaughan, editors, *Advances in Neural Information Processing Systems 34: Annual Conference on Neural Information Processing Systems 2021, NeurIPS 2021, December 6-14, 2021, virtual*, pages 7207–7219, 2021.
- [54] Chaoyang Wang and Simon Lucey. Paul: Procrustean autoencoder for unsupervised lifting. In *Proceedings of the IEEE/CVF Conference on Computer Vision and Pattern Recognition*, pages 434–443, 2021.
- [55] Shangzhe Wu, Christian Rupprecht, and Andrea Vedaldi. Unsupervised learning of probably symmetric deformable 3d objects from images in the wild (extended abstract). In Zhi-Hua Zhou, editor, *Proceedings of the Thirtieth International Joint Conference on Artificial Intelligence, IJCAI 2021, Virtual Event / Montreal, Canada, 19-27 August 2021*, pages 4854–4858. ijcai.org, 2021.
- [56] Yu Xiang, Roozbeh Mottaghi, and Silvio Savarese. Beyond PASCAL: A benchmark for 3d object detection in the wild. In *IEEE Winter Conference on Applications of Computer Vision, Steamboat Springs, CO, USA, March 24-26, 2014*, pages 75–82. IEEE Computer Society, 2014.
- [57] Heng Yang and Luca Carlone. In perfect shape: Certifiably optimal 3d shape reconstruction from 2d landmarks. In *Proceedings of the IEEE/CVF Conference on Computer Vision and Pattern Recognition*, pages 621–630, 2020.
- [58] Zi Jian Yew and Gim Hee Lee. 3dfeat-net: Weakly supervised local 3d features for point cloud registration. In *European Conference on Computer Vision*, pages 630–646. Springer, 2018.
- [59] Stefanos Zafeiriou, Grigorios G Chrysos, Anastasios Roussos, Evangelos Ververas, Jiankang Deng, and George Trigeorgis. The 3d menpo facial landmark tracking challenge. In *Proceedings of the IEEE International Conference on Computer Vision Workshops*, pages 2503–2511, 2017.
- [60] Haitian Zeng, Yuchao Dai, Xin Yu, Xiaohan Wang, and Yi Yang. Pr-rnn: Pairwise-regularized residual-recursive networks for non-rigid structure-from-motion. In *Proceedings of the IEEE/CVF International Conference on Computer Vision*, pages 5600–5609, 2021.
- [61] Wanqing Zhao, Shaobo Zhang, Ziyu Guan, Wei Zhao, Jinjie Peng, and Jianping Fan. Learning deep network for detecting 3d object keypoints and 6d poses. In *Proceedings of the IEEE/CVF Conference on Computer Vision and Pattern Recognition*, pages 14134–14142, 2020.
- [62] Xiaowei Zhou, Menglong Zhu, Spyridon Leonardos, Konstantinos G. Derpanis, and Kostas Daniilidis. Sparseness meets deepness: 3d human pose estimation from monocular video. In *2016 IEEE Conference on Computer Vision and Pattern Recognition, CVPR 2016, Las Vegas, NV, USA, June 27-30, 2016*, pages 4966–4975. IEEE Computer Society, 2016.
- [63] Yingying Zhu, Dong Huang, Fernando De la Torre, and Simon Lucey. Complex non-rigid motion 3d reconstruction by union of subspaces. In *2014 IEEE Conference on Computer Vision and Pattern Recognition, CVPR 2014, Columbus, OH, USA, June 23-28, 2014*, pages 1542–1549. IEEE Computer Society, 2014.
- [64] Yi Zhu, Zhongyue Zhang, Chongruo Wu, Zhi Zhang, Tong He, Hang Zhang, R Manmatha, Mu Li, and Alexander Smola. Improving semantic segmentation via self-training. *arXiv preprint arXiv:2004.14960*, 2020.
- [65] Barret Zoph, Golnaz Ghiasi, Tsung-Yi Lin, Yin Cui, Hanxiao Liu, Ekin Dogus Cubuk, and Quoc Le. Rethinking pre-training and self-training. *Advances in neural information processing systems*, 33:3833–3845, 2020.
- [66] Yuliang Zou, Zizhao Zhang, Han Zhang, Chun-Liang Li, Xiao Bian, Jia-Bin Huang, and Tomas Pfister. Pseudoseg: Designing pseudo labels for semantic segmentation. *arXiv preprint arXiv:2010.09713*, 2020.

9. Piecewise Planar Hulls

In this section, we provide more details about the PPH. The important rules for defining PPHs are: (i) each point has to appear in at least one plane and (ii) no two planes should intersect except possibly along their shared edges. Note that in this sentence intersection in 3D is meant and their 2D projections are of course allowed to overlap. The PPHs should ideally be defined such that each plane corresponds to a clear semantically distinguishable surface. This is important for the performance of the semantic segmentation network. For most object classes, this is naturally satisfied since the keypoints are semantically meaningful to begin with.

Another important aspect is the symmetric planes. For example, left and right sides of the car are symmetric and if only the surfaces are considered identical. However, the methods can identify the left and right through referencing on the unique planes such as the front window of the car. In order to facilitate this, we use Coordinate convolutions CoordConv [28]. CoordConv creates a grid of 2D locations and concatenate this grid with the input feature map. The convolution operation is then applied on this concatenated representation. In our setting, this is important to enable the model have a geometric and spatial reasoning.

In order to demonstrate the PPH selection process we followed, we present the PPHs of some classes in Figures 8, 9 and 10. For chair and table classes the semantic meanings of the keypoints results in a somewhat obvious definition of PPHs. Table class has an interesting definition of keypoints in the Pascal dataset. Depending on the table being round or not, the corners of the table changes. Therefore there are 4 keypoints that only apply to round tables and there are 4 tables which only applies to rectangular tables. This does not cause any problems in our framework since we operate on the defined keypoints and we set different planes for round and rectangular tables. Therefore, the method can create both round and rectangular estimates for a rectangular table but we will only consider the rectangular estimates by using the defined keypoints. The bicycle class has some freedom in the definition of the PPH. As it can be seen that, we opted for a large area that represents the side of the bike. We will later show the effects on the performance if we divide this large area into smaller pieces.



Figure 8. PPH of chair.

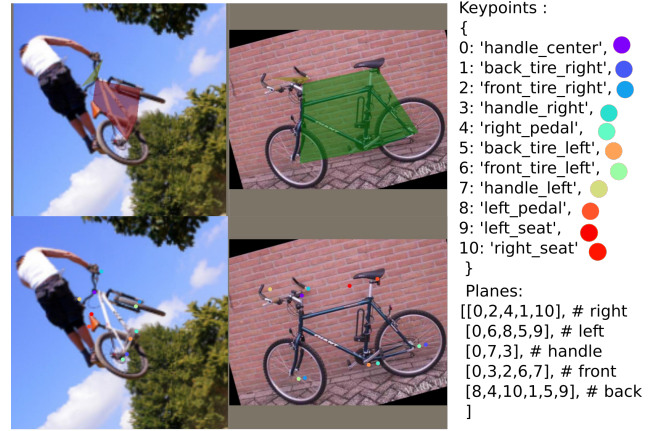


Figure 9. PPH of bicycle.

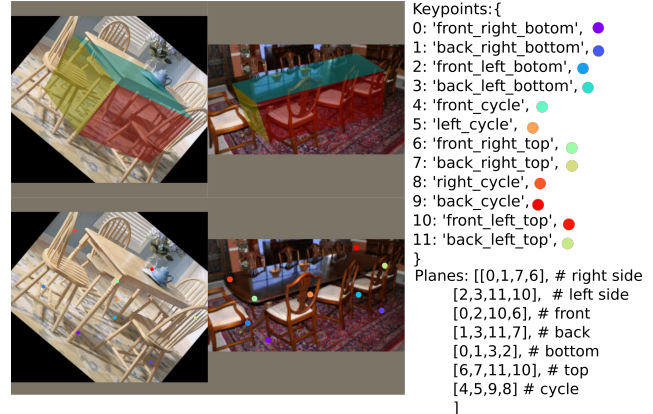


Figure 10. PPH of table.

10. Architecture

The overall architecture has 3 main parts: the transformer, the segmentation network and the 2D-3D (lifter) network. The overall network is given in 11.

The lifter network is identical to C3DPO [34] as men-

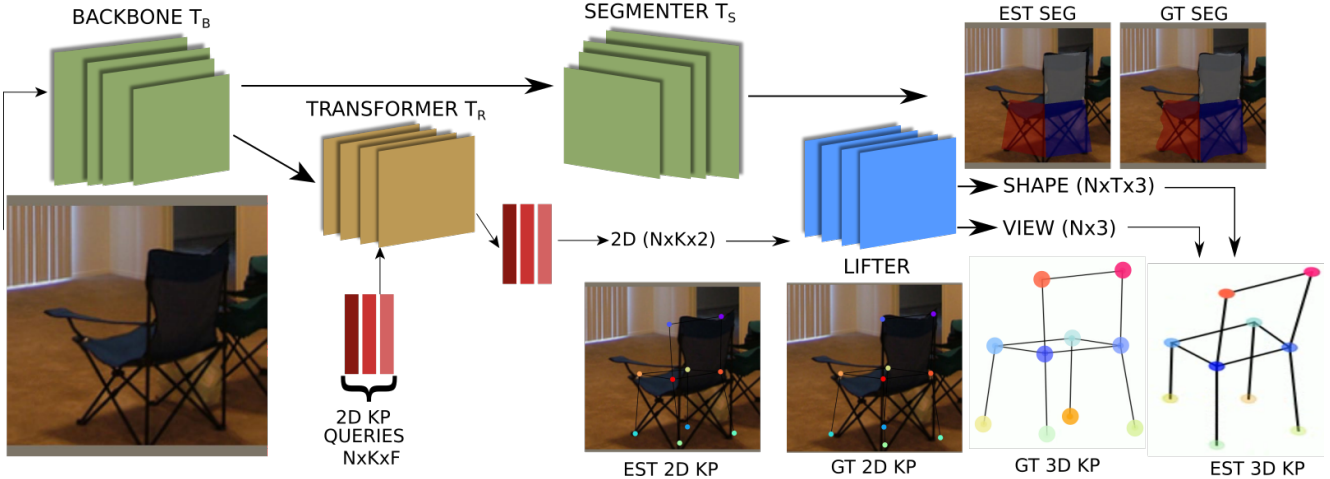


Figure 11. Architecture

tioned in the main paper. The segmentation network is given in Fig 12. It can be seen that the architecture is very simple and uses the intermediate representations of the backbone network. We use 2 iterations and the resulting feature map is 1/4 of the input image. The resulting segmentation logits are obtained by bilinear upsampling with a scale factor of 4.

In Fig 12 righthand side, the residual block we used in segmentation network can be seen. We use CoordConv [28] in our residual blocks. In order to improve the performance of the segmentation, we use the intermediate representations of the Resnet50 backbone network as skip connections. The skip connections are processed by a residual block and then added with the representation from the lower level. The new feature map is upscaled by a factor of $x2$. In total, the resulting feature map is 1/4 of the input image. We use bilinear upsampling with a factor $x4$ to obtain the final segmentation logits.

11. Ablations

A natural question to ask is the dependence of the framework on the different definitions of the PPHs. While for most closed convex objects such as cars, bus, sofa etc. the definition is somewhat ubiquitous, for some other categories like bicycle and airplane, the definitions mostly depend on the annotator. Here we present our results when the PPH definitions of bicycle and airplane are different than the ones we used in the main paper.

The differences between the paper versions of the PPH and ablation are given in Fig 13 and 14. In both cases, we divide the large surfaces into smaller segments. The resulting structure has more plane than the PPHs we used in the paper.

In Table 4, we present the 3D results of the ablated version with an asterisk. It can be seen that the results are very

similar to each other on average. This shows that the performance of the framework does not depend on the PPH definitions very much. In table 6, we present the performance of the ablation network on 2D keypoint estimation task. The results are again very close to each other.

In Table 5, we specifically focus on the two changed categories and investigate the performance differences in the original and ablated versions. In bicycle class, we see a very slight improvement in performance with the ablation version of the PPH, albeit the improvement is too small to be considered significant. In the airplane class, the results are mixed and on average there does not seem to be a clear difference between the original and ablations versions.

In Fig 15, we investigate the convergence behavior of the proposed method with the original PPHs. In the paper, we present results with 3 recursions. The reason for this choice is that the performance saturates after 3 recursions. In order to demonstrate this, we present the performance over 4 recursions. It can be seen that MPJPE results simply converge after 3 recursions and while there is some fluctuation in 2D of the 5% model, generally, the 2D performance of the models also saturate around 3 recursions. Considering each recursion costs 2 GPU days, 3 recursion is the optimal cut-off point.

12. Additional Results

Apart from the visual results we presented in the paper, we present additional visual results. In Fig 16, it can be seen that the framework achieves its goal of improving the performance of the model with every recursion. On top row, we see that the depth of the TV screen is clearly increasing with each recursion and approaching the GT 3D shape. In middle row, The slight worsening in the recursion 2 is then fixed

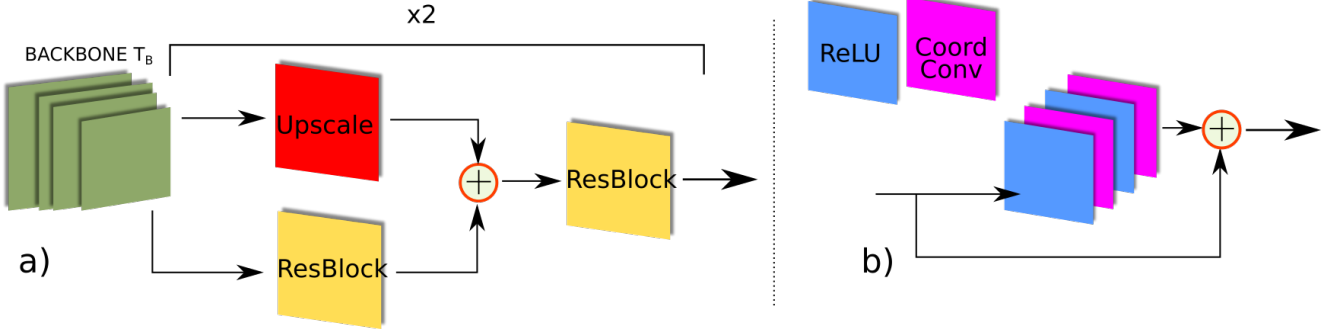
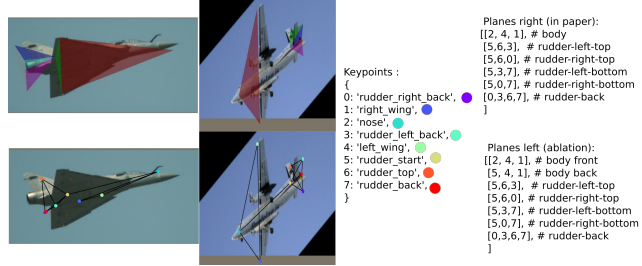


Figure 12. Segmentation network. a) The intermediate representations of the backbone are used to iteratively upscale and refine the feature maps. b) The residual block we use is made up of CoordConv and ReLU non-linearity.

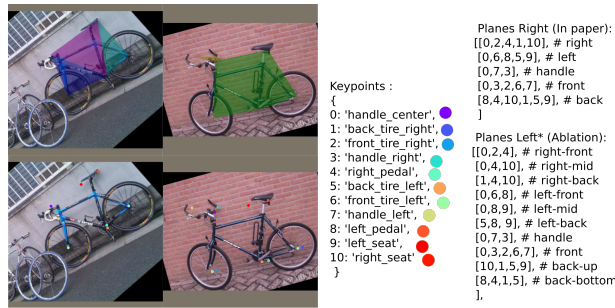
Method	C3DPO/SH†				Ours				Ours*			
	5	10	50	100	5	10	50	100	5	10	50	
MPJPE	86.3	79.6	77.2	57.4	85.6	76.3	68.7	51.6	85.5	75.1	68.9	
Stress	70.1	64.8	59.2	41.4	54.8	52.5	50.9	35.3	55.3	51.0	51.3	

Table 4. Results on Pascal3D. †: 2D keypoint estimator stacked hourglass network is pretrained and further trained using 100% of training data. * Method uses GT 2D keypoints at test time. Ours* is the results with different PPHs than Ours.



Method	Ours			Ours*		
	5	10	50	5	10	50
MPJPE Bike	83.8	49.2	41.4	83.3	48.6	41.3
Stress Bike	26.0	23.5	21.1	21.9	21.7	19.6

Table 5. Results on Pascal3D. †: 2D keypoint estimator stacked hourglass network is pretrained and further trained using 100% of training data. * Method uses GT 2D keypoints at test time. Ours* is the results with different PPHs than Ours.



Method	SH	Ours				Ours*			
		100	5	10	50	100	5	10	50
L2 (All KP)	35.6	49.4	38.3	28.9	28.2	48.6	37.9	29.0	
L2 (Vis KP)	18.6	48.1	37.1	27.3	26.5	47.4	36.4	27.6	

Table 6. Results on Pascal3D for all defined keypoints (All KP) and the visible keypoints (Vis KP). †: 2D keypoint estimator stacked hourglass network is pretrained.

in the following recursion and the performance improved. In the last row, the seat part of the chair is the best in the last recursion. Another observation from the visual results

is the performance of the model that uses all of the training data. It can be seen that 100% data model achieves the best results as expected. These results confirm that the proposed method's validity.

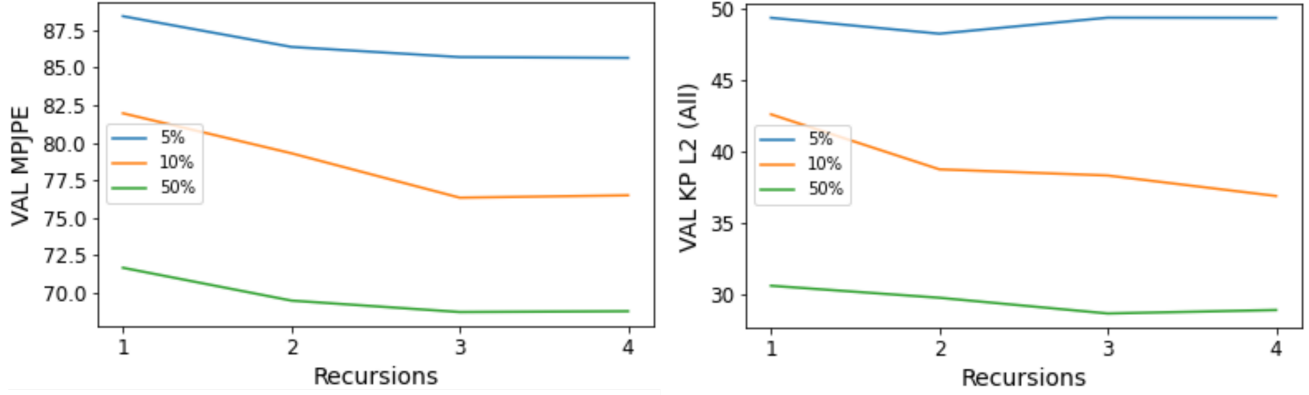


Figure 15. Convergence analysis of the method. MPJPE and L2 metrics on validation set are given. It can be seen that the method converges at around 3 recursions. That is the point, we used the results in our paper.



Figure 16. The results of the proposed method with different data utilization. It can be seen that the performance improve with each recursion.